Journal of Materials Chemistry A

PAPER

View Article Online
View Journal | View Issue

Published on 20 August 2014. Downloaded by University of Tennessee at Knoxville on 10/06/2016 21:53:50.

Cite this: J. Mater. Chem. A, 2014, 2, 17454

Cellulose derived magnetic mesoporous carbon nanocomposites with enhanced hexavalent chromium removal†

Bin Qiu,[ab] Hongbo Gu,[a] Xingru Yan,[ac] Jiang Guo,[ac] Yiran Wang,[a] Dezhi Sun,*[b] Qiang Wang,[b] Mojammel Khan,[d] Xin Zhang,[e] Brandon L. Weeks,[e] David P. Young,[e] Zhanhu Guo*[a] and Suying Wei*[c]

Received 6th August 2014
Accepted 20th August 2014

DOI: 10.1039/c4ta04040f

www.rsc.org/MaterialsA

Magnetic carbon–iron nanoadsorbents fabricated by carbonizing cellulose and reducing Fe_3O_4 nanoparticles or $Fe(NO_3)_3$ (the products are denoted as MC–O and MC–N, respectively) have demonstrated great Cr(VI) removal. MC–N with a higher proportion of zero-valence iron (ZVI) and bigger specific surface area exhibited better resistance to oxygen and acid than MC–O due to its smaller pore size. The Cr(VI) removal was highly pH-dependent. For example, 4.0 mg L^{-1} Cr(VI) neutral solution was completely purified by 2.5 g L^{-1} MC–O and MC–N within 10 min. 1000 mg L^{-1} Cr(VI) solution at pH 1.0 was completely removed by both nanoadsorbents in 10 min. The MC–O nanoadsorbents had a higher removal percentage (98.1%) than MC–N (93.5%) at pH 7.0, while MC–N had a removal capacity of 327.5 mg g^{-1}, much higher than 293.8 mg g^{-1} of MC–O at pH 1.0. A chemical adsorption was revealed from the pseudo-second-order kinetic study. Monolayer adsorption of Cr(VI) was revealed by a better fitting of the Langmuir model isotherm, rather than multilayer adsorption for the Freundlich model. These nanoadsorbents could be easily separated from solution by using a permanent magnet after being treated with Cr(VI). Finally, the Cr(VI) removal mechanisms were proposed considering the Cr(VI) reduction and precipitation of Cr(III).

1. Introduction

Hexavalent chromium (Cr(VI)) is a common contaminant in surface water and groundwater because it is widely used in many industries, including the electroplating, printing, pigments and other areas. Cr(VI) has been classified as one of the most toxic pollutants due to its acute toxicity for living organisms and its potential carcinogenicity for human being.[1] The chromium concentration in water must be reduced to an acceptable level before being discharged into the environment. Chromium usually exists in the Cr(VI) and trivalent Cr(III) forms in aqueous environment.[2] Cr(VI) is more toxic and mobile than Cr(III), and Cr(III) does not readily migrate in solution since it usually precipitates as hydroxides and oxides.[2] Recently, many technologies have been developed to remove Cr(VI) from waste or drinking water, including electrochemical precipitation,[2] ion exchange,[3] membrane separation,[4] photocatalysis[5,6] and adsorption.[7–9] Among these techniques, adsorption has been widely used due to its great removal performance and easy operation.[10–12] Considering the easier removal of Cr(III), the combination of Cr(VI) reduction to Cr(III) and subsequent adsorption of Cr(III) has been demonstrated effective for Cr(VI) removal.[13–15] Among various adsorbents, magnetic carbon attracts increasing interest due to its fast removal rate and easy separation property under an external magnetic field. Magnetic carbons have been fabricated by pyrolysis,[16] the microwave assisted pyrolysis method,[17] and the hydrothermal carbonization method.[18] It has been widely used as the adsorbent for the removal of heavy metal ions and organics from aqueous solution. The carbon layer prevents iron dissolving in the acidic solutions,[19] leading to a longer life of the adsorbents. Meanwhile, the carbon matrix protects iron against oxidation once it was exposed to air.[20–22] As an important active component in the magnetic carbon adsorbents, iron mainly includes Fe_3O_4, Fe_2O_3 and zero-valence iron (ZVI).[16,17,23] ZVI demonstrates a greater performance on Cr(VI) removal because it can provide more electrons for the Cr(VI) reduction.[24,25]

[a]Integrated Composites Laboratory (ICL), Dan F Smith Department of Chemical Engineering, Lamar University, Beaumont, TX 77710, USA. E-mail: zhanhu.guo@lamar.edu

[b]College of Environmental Science and Engineering, Beijing Forestry University, Beijing, 100083 China. E-mail: sundezhi@bjfu.edu.cn

[c]Department of Chemistry and Biochemistry, Lamar University, Beaumont, TX 77710, USA. E-mail: suying.wei@lamar.edu

[d]Department of Physics and Astronomy, Louisiana State University, Baton Rouge, LA 70803, USA

[e]Department of Chemical Engineering, Texas Technology University, Lubbock, TX 79409, USA

† Electronic supplementary information (ESI) available. See DOI: 10.1039/c4ta04040f

This journal is © The Royal Society of Chemistry 2014

Published on 20 August 2014. Downloaded by University of Tennessee at Knoxville on 10/06/2016 21:53:50.

The iron precursor is of importance for preparing magnetic carbon adsorbents, including Fe_3O_4 nanoparticles[20] and Fe^{3+} ions.[26] Meanwhile, the carbon precursor is important for the reduction of Fe(III) to ZVI and formation of carbon during its carbonization process, such as polymer,[20] furfuryl alcohol,[27] rice husk[28] and cotton fabric.[26] The Fe_3O_4/carbon core–shell structure has been fabricated by using Fe_3O_4 and polyaniline as the iron and carbon precursors through calcination at 750 °C.[20] Zhu *et al.*[26] reported a magnetic carbon fabric synthesized by using cotton fabric as the carbon precursor *via* microwave assisted heating at 750 °C. The result shows that partial Fe^{3+} was reduced to ZVI during the calcination of cotton fabric. Cellulose, an abundant and sustainable carbon precursor in nature, has been considered as a renewable and advanced material for the preparation of carbon.[29–31] Moreover, hydrogen and other reductive intermediates, such as carbon monoxide and carbon, can be produced during its pyrolysis process at high temperatures,[32,33] which can reduce the Fe(III)/Fe(II) species to ZVI. However, the preparation of novel magnetic carbon nanoadsorbents with a high proportion of ZVI with cellulose as the carbon precursor and their application for Cr(VI) have not been reported yet.

In this study, magnetic carbon nanoadsorbents were fabricated by using cellulose as the carbon source through a simple calcination method. The effects of iron precursors including the Fe_3O_4 nanoparticle and $Fe(NO_3)_3$ on the properties of the synthesized magnetic carbons and their performances on Cr(VI) removal were studied. The effects of solution pH, treatment time and Cr(VI) concentration on the Cr(VI) removal performance were investigated. Meanwhile, the Cr(VI) removal kinetics and isothermal behaviors were studied to disclose the Cr(VI) removal rate and maximum removal capability of the magnetic carbon nanoadsorbents. The mechanisms involved in the Cr(VI) removal with different pH values were determined to reveal the Cr(VI) removal nature of the magnetic carbon nanoadsorbents.

2. Methods and materials

2.1. Materials

Cellulose and $Fe(NO_3)_3\cdot 9H_2O$ were purchased from Sigma Aldrich. Potassium dichromate ($K_2Cr_2O_7$), 1,5-diphenylcarbazide (DPC) and ethanol were purchased from Alfa Aesar Company. Phosphoric acid (H_3PO_4, 85 wt%) was obtained from Fisher Scientific. The Fe_3O_4 nanoparticles with an average diameter of 40 nm were purchased from Nanjing Emperor Nano Material Co., Ltd., China. All the chemicals were used as received without any further purification.

2.2. Fabrication of magnetic carbon nanoadsorbents

The magnetic carbon nanoadsorbents were fabricated by calcination. Briefly, 12.0 g $Fe(NO_3)_3\cdot 9H_2O$ was dissolved in 50 mL ethanol, in which 12.0 g cellulose was added. The mixed suspension was mechanically stirred at 300 rpm for 2 h at room temperature and $Fe(NO_3)_3$ was homogeneously distributed within cellulose. The well-mixed suspension was then heated in a water bath at 50 °C to completely evaporate ethanol. The remaining solid ($Fe(NO_3)_3$/cellulose) was dried in a vacuum oven overnight. The $Fe(NO_3)_3$/cellulose was loaded in a tube furnace and was heated to 800 °C at a heating rate of 10 °C min^{-1} under nitrogen conditions. Then the temperature was decreased naturally to room temperature. These magnetic carbon nanoadsorbents were named as MC–N. The same processes were done for the fabrication of magnetic carbon nanoadsorbents derived from the Fe_3O_4 nanoparticles. Briefly, 3.84 g Fe_3O_4 nanoparticles (equal iron mole to $Fe(NO_3)_3\cdot 9H_2O$) were used as the iron precursor. The preparation procedures were the same as mentioned above. These magnetic carbon nanoadsorbents were named as MC–O.

2.3. Cr(VI) removal experiments

The effects of initial Cr(VI) concentration on Cr(VI) removal efficiency were investigated by using magnetic carbon nanoadsorbents (50.0 mg) to treat Cr(VI) solutions (20.0 mL) at pH = 7.0 with Cr(VI) concentration ranging from 1.0 to 10.0 mg L^{-1} for 30 min. The effects of the solution pH value on Cr(VI) removal by magnetic carbon nanoadsorbents were investigated with an initial pH value of 1.0, 2.0, 3.0, 5.0, 7.0, 9.0 and 11.0. The pH of Cr(VI) solutions was adjusted using NaOH (1.0 mol L^{-1}) and H_2SO_4 (1.0 mol L^{-1}) with a pH meter (Vernier Lab Quest with pH-BTA sensor). The magnetic carbons (50.0 mg) were added into 20.0 mL Cr(VI) solutions (4.0 mg L^{-1}). The pH values and Cr(VI) concentrations in solutions were measured at different interval times. For kinetic study, the synthesized magnetic carbons were used to treat 1000 and 20.0 mg L^{-1} Cr(VI) solution (20.0 mL) at initial pH 1.0 and 7.0, respectively. The Cr(VI) concentrations that remained in solutions were measured at different interval times. For comparison, the synthesized carbon nanoadsorbents (50.0 mg) and the as received Fe_3O_4 nanoparticles (50 mg) were also used to treat 4.0 mg L^{-1} Cr(VI) solution (20.0 mL) at pH 7.0 for 10 min. All the Cr(VI) removal tests were conducted at room temperature.

The Cr(VI) concentration in solution was determined by the colorimetric method[7] by using the obtained standard fitting equation: $A = 9.7232 \times 10^{-4}C$, where C is the concentration of Cr(VI) and A is the absorbance at 540 nm obtained from the UV-vis test. The Cr(VI) removal percentage (R%) is calculated using eqn (1):

$$R\% = \frac{C_0 - C_e}{C_0} \times 100\% \quad (1)$$

where C_0 and C_e (mg L^{-1}) are the Cr(VI) concentrations in solution before and after treatment, respectively. The removal capacity (Q, mg g^{-1}) is quantified by eqn (2):

$$Q = \frac{(C_0 - C_e)V}{m} \quad (2)$$

where V (L) represents the volume of Cr(VI) solution and m (g) is the mass of the used magnetic carbon nanoadsorbents.

2.4. Characterization

The morphology of the fabricated magnetic carbons was characterized by scanning electron microscopy (SEM, Hitachi

Published on 20 August 2014. Downloaded by University of Tennessee at Knoxville on 10/06/2016 21:53:50.

S4300). All the samples were sputter coated with a thin layer of gold (about 5 nm) to ensure good conductivity. The powder XRD analysis of the samples was carried out with a Bruker AXS D8 Discover diffractometer with GADDS (General Area Detector Diffraction System) operating with a Cu-Kα radiation source filtered with a graphite monochromator (λ = 1.5406 Å). The specific Brunauer–Emmett–Teller (BET) surface area and pore size distribution were measured on a Quanta chrome Nova 2200e by nitrogen adsorption at 77.4 K. Prior to each measurement, the synthesized magnetic carbon samples were degassed at 300 °C for 12 h under high vacuum (<0.01 mbar). The pore size distribution of the samples was calculated by the Barrett–Joyner–Halenda (BJH) method using nitrogen desorption isotherms. The X-ray photoelectron spectroscopy (XPS) measurements were performed in a Kratos AXIS 165 XPS/AES instrument using monochromatic Al Kα radiation to check the elemental compositions. The Cr2p, Fe2p, C1s and O1s peaks were deconvoluted into the components consisting of a Gaussian/Lorentzian line shape function (Gaussian = 80%, Lorentzian = 20%) on linear background.

The magnetic property measurements were carried out in a 2 T physical property measurement system (PPMS) by Quantum Design at room temperature.

3. Results and discussion

3.1. Magnetic carbons

The SEM images of the MC–O (Fig. 1A) show the spherical particles with an average diameter of ~100 nm. However, bigger particles with an average diameter of 500 nm are observed in the MC–O as well, indicating the aggregation of the Fe_3O_4 nanoparticles during the carbonization of cellulose. The smaller magnetic carbon particles are distributed loosely on the surface of bigger particles. The MC–N presents the spherical particles. The particle size is centered at ~250 nm (Fig. 1B), which is much larger and more homogeneous than the MC–O. The XRD characterizations were conducted to reveal the crystalline structure of iron in MC–O and MC–N. Fig. 1C shows the wide-angle XRD patterns of the MC–O and MC–N fabricated at 800 °C. The diffractions at 30.1°, 35.5°, 56.9° and 62.6° in the spectra of MC–O (Fig. 1C(c)) correspond to the (220), (311), (511) and (440) reflections of Fe_3O_4,[26] respectively. The diffractions at 25.6°, 44.7°, 45.0° and 65.0° are indexed to the (002), (100), (110) and (200) planes of cubic Fe,[26] respectively. The high intensity ratio of Fe to Fe_3O_4 demonstrates that most of Fe_3O_4 has been reduced to ZVI by the intermediates of cellulose during calcination at 800 °C. Similar results are also observed for the MC–N (Fig. 1C(a)). However, a higher intensity ratio of Fe to Fe_3O_4 shows that the MC–N has a higher portion of ZVI than MC–O. As reported, the Fe^{3+} can also be partly reduced to ZVI by the calcination of rice husk[28] and cotton fabric[26] with a calcination temperature of 850 °C. The reductive intermediates, *e.g.* hydrogen, carbon monoxide and carbon, were generated during the decomposition of cellulose at high temperature,[32,33] which caused the reduction of Fe^{3+} to ZVI. As documented in the literature, ZVI presents a superior performance on Cr(VI) reduction from polluted solutions.[24,25] Therefore, the cellulose is demonstrated as a good carbon precursor to fabricate the ZVI magnetic carbon nanoadsorbents.

The specific surface area and pore size distribution are important properties of the adsorbents, which determine the pollutants' transfer between wastewater and the adsorbents. The nitrogen adsorption–desorption isotherms of the MC–O (Fig. 1D(a)) and MC–N (Fig. 1D(b)) show the representative type-IV curves with the hysteresis loops, demonstrating the mesoporous properties of the MC–O and MC–N. The porous

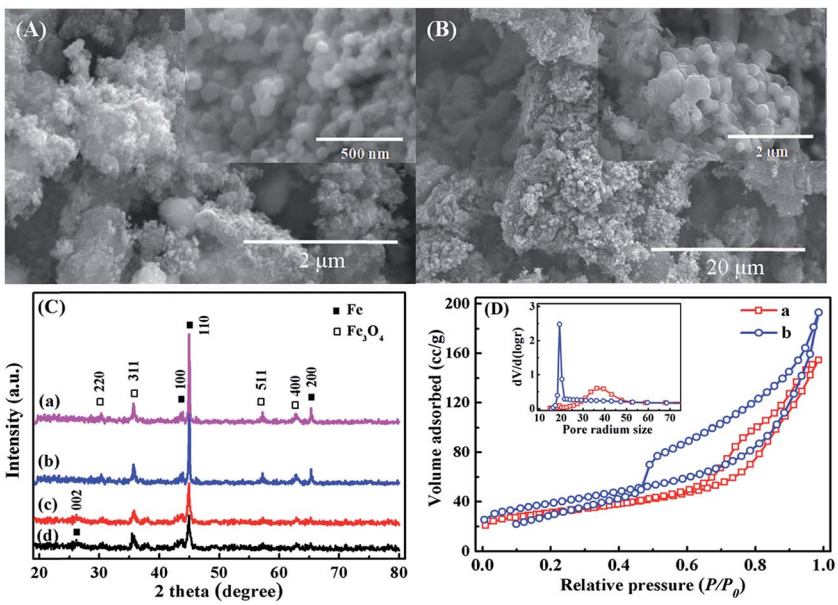

Fig. 1 SEM images of (A) MC–O and (B) MC–N; (C) XRD profiles of MC–N (a) before and (b) after storage in air for one week, and MC–O (c) before and (d) after storage in air for one week; (D) nitrogen adsorption–desorption isotherms and pore size distributions of (a) MC–O and (b) MC–N.

 This journal is © The Royal Society of Chemistry 2014

Published on 20 August 2014. Downloaded by University of Tennessee at Knoxville on 10/06/2016 21:53:50.

structures of the magnetic carbons are summarized in Table 1. The specific surface areas of the MC–O and MC–N are 111.4 and 136.27 $m^2\ g^{-1}$, respectively. Both the magnetic carbon nanoadsorbents have much larger specific surface area than the Fe_3O_4 nanoparticles (89.78 $m^2\ g^{-1}$) (Fig. S1†), suggesting that the carbon packed on the surface significantly has enlarged the specific surface area of the magnetic nanoparticles. It is observed that the MC–N has a much larger specific surface area than the MC–O, indicating that iron nitrate is better for the fabrication of magnetic carbon nanoadsorbents. The produced volatile NO gas during the decomposition of nitrate produced more pores. The BJH pore size distribution calculated from the desorption branch is shown in Fig. 1D (inset). The wide pore radius size ranging from 30 to 50 Å is observed for the MC–O, much smaller than that of the as-received Fe_3O_4 nanoparticles with a pore radium size of 42.95 Å (Fig. S1†). However, the pore radius size of MC–N is centered at 19.2 Å with a narrow size distribution, indicating the mesoporous property with a pore diameter of 38.4 Å. The pore of MC–N is much smaller and more homogeneous than that of MC–O, consistent with the results observed in SEM (Fig. 1A and B). The more homogeneous distribution of $Fe(NO_3)_3$ solution in cellulose contributes to the homogeneous particle distribution and uniform pore size of the MC–N. It indicates that $Fe(NO_3)_3$ is a better iron precursor for the synthesis of the ZVI magnetic carbon nanoadsorbents.

The oxygen resistance is an important property of the ZVI magnetic carbon nanoadsorbents. In this study, the oxygen resistance of MC–O and MC–N was determined by exposing them in air for 1 week. The iron forms in the exposed MC–O and MC–N were determined by XRD (Fig. 1C(b and d)). The intensity portion of Fe_3O_4 in the MC–O is observed to be increased (Fig. 1C(d)) compared to the synthesized MC–O, suggesting that ZVI has been oxidized. However, no obvious change is observed in the XRD patterns of the exposed MC–N with a little increase in Fe_3O_4 intensity (Fig. 1C(b)), showing that the MC–N is more stable against the oxidation by air. The structure differences are attributed to different pore structures of the magnetic carbons. The looser structure and larger pore size of the MC–O (Fig. 1A) facilitate the oxygen transfer into the particles, leading to easy oxidation of ZVI. While the tight structure and smaller pore size (Fig. 1D(b)) contribute to the high resistance of the MC–N against the oxygen diffusion and oxidation of ZVI.

3.2. Cr(VI) removal

Fig. 2A shows the Cr(VI) removal percentages by different adsorbents from the contaminant solutions with an initial pH of 7.0. The adsorbent concentration was maintained at a constant value of 2.5 $g\ L^{-1}$ and a short treatment time of 10 min was employed in this study. The CM–O can completely remove 4.0 $mg\ L^{-1}$ Cr(VI) within 10 min, while 98% of Cr(VI) was removed by CM–N. Only 25% and 27% of Cr(VI) removal percentages were achieved by the as-received Fe_3O_4 nanoparticles and cellulose, respectively. This result revealed the superior performances of the MC–O and MC–N on Cr(VI) removal over Fe_3O_4 and cellulose.

Table 1 BET specific surface area and pore size of the MC–O, MC–N and Fe_3O_4 based on the nitrogen adsorption–desorption isotherm

Samples	MC–O	MC–N	Fe_3O_4
BET surface area ($m^2\ g^{-1}$)	111.44	136.27	89.78
Average pore radius size (Å)	36.409	19.203	42.95
Micropore volume (cc g^{-1})	0.010	0.034	0.004
Mesopore volume (cc g^{-1})	0.229	0.265	0.325

Fig. 2B shows the Cr(VI) removal performance with different Cr(VI) concentrations by MC–O and MC–N at pH 7.0. 4.0 and 3.0 $mg\ L^{-1}$ Cr(VI) were totally removed by 2.5 $g\ L^{-1}$ MC–O and MC–N in 10 min, respectively. The removal percentages then decreased with the increase in Cr(VI) concentrations. The decreases in Cr(VI) removal percentages are mainly due to the limitation of active adsorption sites on the surface of the adsorbents. However, more than 80% Cr(VI) can be removed by both the magnetic adsorbents in 10 min even when the initial Cr(VI) concentration is up to 10.0 $mg\ L^{-1}$. Moreover, the MC–O presents a little better performance on Cr(VI) removal than MC–N with a little higher Cr(VI) removal percentage. The bigger pore size of MC–O (Fig. 1D) may improve the Cr(VI) diffusion into the internal particles and facilitate the reduction reaction between the electron donors (ZVI) and Cr(VI).

The pH value is one of the most important variables affecting the Cr(VI) removal property. Fig. 2C shows the Cr(VI) removal percentages by the MC–O and MC–N with initial pH ranging from 1.0 to 11.0. The complete Cr(VI) removal was achieved with pH ranging from 1.0 to 5.0 with 10 min, while a significant decrease in the Cr(VI) removal percentage was observed in basic solutions. ~70% Cr(VI) can be removed from the solution with a pH of 11.0. The synthesized magnetic carbons perform the Cr(VI) removal as well as the magnetic carbon fabricated by the microwave assisted heating method.[26] The MC–O has a little higher Cr(VI) removal percentage than the MC–N from the neutral and basic solutions. Indeed, Cr(VI) was totally removed by both the MC–O and MC–N within several minutes at pH 1.0 and 2.0.Therefore, the Cr(VI) removal performances by both the MC–O and MC–N were further determined with a high Cr(VI) concentration of 1000 $mg\ L^{-1}$ (Fig. 2D). Both the MC–O and MC–N can completely remove the 1000 $mg\ L^{-1}$ Cr(VI) from the solutions at a pH of 1.0 in 10 min. It demonstrated much fast removal rates and high removal capacities of the MC–O and MC–N. There are two possible reasons for a high Cr(VI) removal rate by the magnetic carbons in acidic solutions. One is that the magnetic carbons are favorable to remove $HCrO_4^-$ rather than CrO_4^{2-}. As documented, the most important forms of Cr(VI) in aqueous solution are chromate (CrO_4^{2-}), dichromate ($Cr_2O_7^{2-}$) and hydrogen chromate ($HCrO_4^-$ and H_2CrO_4) and these ion forms are related to the solution pH and the total Cr concentration.[13] $HCrO_4^-$ is the dominant form when the pH is lower than 6.8, while only CrO_4^{2-} is stable when the pH is above 6.8.[13] $HCrO_4^-$ with a higher redox potential (1.33 V) can be easily reduced to Cr(III) by ZVI, which acts as the electron donor. The electrostatic attraction between the negatively charged Cr(VI) ions and the positively charged adsorbents under acidic conditions is another possible reason. Moreover, ZVI was dissolved by the acidic solution and produces the reductive

Published on 20 August 2014. Downloaded by University of Tennessee at Knoxville on 10/06/2016 21:53:50.

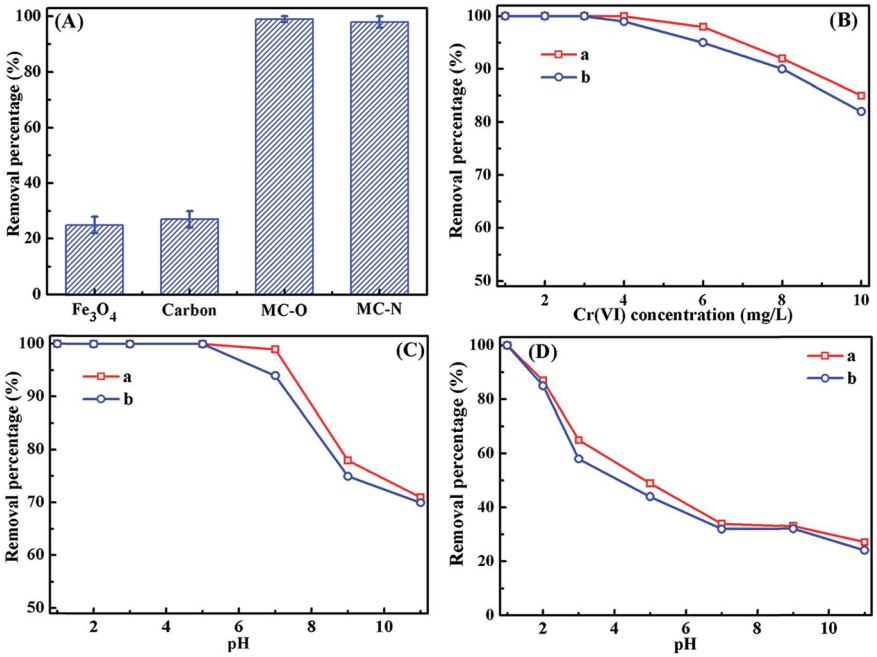

Fig. 2 (A) Cr(VI) removal performance of different adsorbent (Cr(VI) concentrations: 4.0 mg L^{-1}, pH = 7.0, adsorbent dosage: 50.0 mg, volume: 20 mL, treating time: 10 min); (B) effect of initial Cr(VI) concentration on Cr(VI) removal performance (adsorbent dosage: 50.0 mg, volume: 20 mL, pH: 7.0, treating time: 10 min); and the effect of solution pH on the Cr(VI) removal performance by (a) MC–O and (b) MC–N with the initial Cr(VI) concentration of (C) 4.0 and (D) 1000 mg L^{-1} (adsorbent dosage: 50.0 mg, volume: 20.0 mL, treating time: 10 min).

intermediates such as $H^{\bullet}$, hydrogen and Fe^{2+}, which can also act as the electron donors for the reduction of Cr(VI) to Cr(III). The H_2 gas bubble can be observed on the surface of adsorbents when they were added into the solution with an initial pH of 1.0, indicating the corrosion of ZVI. Generally, ZVI plays an important role in Cr(VI) removal by donating the electrons for Cr(VI) reduction. During the Cr(VI) reduction, the solution pH was increased obviously (Fig. S2†), compared to that before treatment, which supports that the protons were consumed for the production of reductive intermediates.

3.3. Removal kinetics and isotherms

The Cr(VI) removal by both the MC–O and MC–N was rapid during the initial reaction stage, and then became gradually slow. A similar kinetics was also observed in Cr(VI) adsorption by the magnetic carbons prepared by using the rice husk[28] and cotton fabric[26] as the carbon sources. Similar phenomena were also observed for other adsorbents such as the Fe_3O_4 core–shell carbon[20] and polymers, such as the polyethylenimine functionalized granules.[13] In this study, the Cr(VI) removal kinetics by the MC–O and MC–N were investigated with an initial pH of 7.0 and 1.0. The Cr(VI) adsorption reached an equilibrium within 20 min with an initial pH of 7.0. More importantly, ~60% Cr(VI) could be removed in 5 min, Fig. 3A and B. The removal rate from the solution with a pH of 1.0 is much faster than that from a solution with a pH of 7.0. The adsorption processes by both MC–O and MC–N nanoadsorbents are found to fit better with the pseudo-second-order model, Fig. 3A and B. The better fitting with pseudo-second-order kinetics reflects that the adsorption rates are controlled by the chemical sorption.[13] The Cr(VI) removal rates by the MC–O are a little faster than those by the MC–N, mainly due to its larger pore size. The time for the complete Cr(VI) removal by the MC–O and MC–N is much shorter than that by the active carbon (6 h),[34] and aerobic granules grafted with polyethylenimine (3 h).[13]

Different equilibrium models are often used to fit the adsorption behavior of an adsorbent. The equilibrium data for Cr(VI) removal by the MC–O and MC–N were fitted by Langmuir[35] and Freundlich[36] models in this study, respectively. The Langmuir isotherm was described as eqn (5):

$$\frac{C_e}{q_e} = \frac{1}{bq_{max}} + \frac{C_e}{q_{max}} \quad (3)$$

where C_e (mg L^{-1}) is the equilibrium Cr(VI) concentration, q_e (mg g^{-1}) is the Cr(VI) amount adsorbed at equilibrium, q_{max} (mg g^{-1}) is the adsorption capacity of adsorbents and b (L mg^{-1}) is a constant. The Freundlich isotherm is an empirical model that considers heterogeneous adsorptive energies on the surface of the absorbent, and can be described as eqn (4);

$$\log q_e = \log k_f + \frac{1}{n} \log C_e \quad (4)$$

where q_e (mg g^{-1}) is the amount of Cr(VI) adsorbed on the surface of adsorbents at equilibrium and k_f and n are constants of the Freundlich model.

The Cr(VI) adsorption isotherms by the MC–O and MC–N were conducted at the initial pH of 7.0, and were fitted by the Langmuir and Freundlich models, Fig. 3C and D. According to the correlation coefficient values, it can be found that the Cr(VI)

 This journal is © The Royal Society of Chemistry 2014

Published on 20 August 2014. Downloaded by University of Tennessee at Knoxville on 10/06/2016 21:53:50.

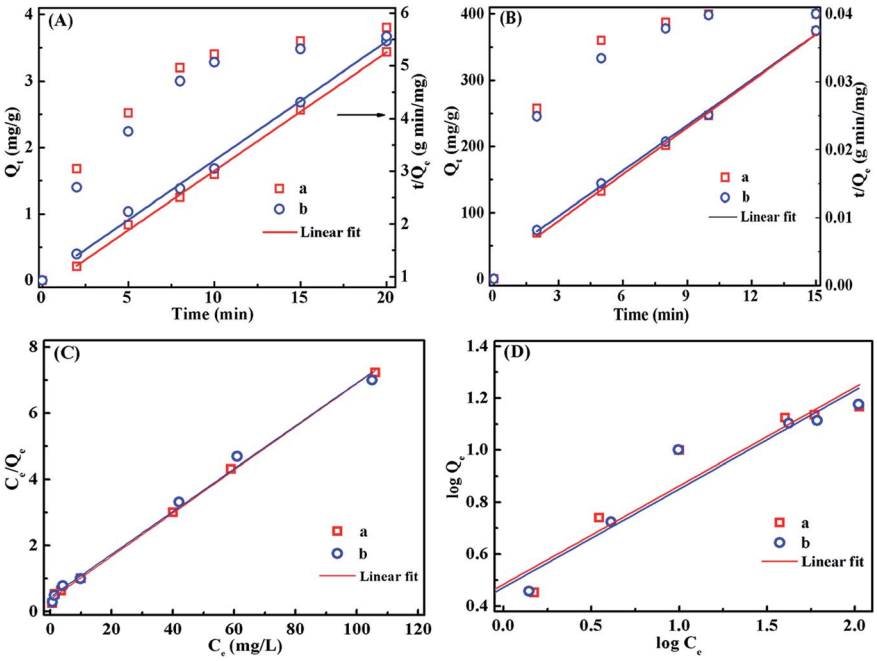

Fig. 3 Cr(VI) adsorption kinetics by (a) MC–O and (b) MC–N fitted by pseudo-second-order models at pH (A) 7.0 and (B) 1.0; the Cr(VI) adsorption isotherm by (a) MC–O and (b) MC–N fitted by (C) Langmuir and (D) Freundlich models.

adsorption isotherm by both the MC–O and MC–N fits better with the Langmuir model, indicating that the Cr(VI) adsorption by the magnetic carbons is limited by the monolayer coverage.[35] The calculated maximum Cr(VI) removal capacity from the Langmuir model for the MC–O at a pH of 7.0 is 15.3 mg g^{-1}, a little higher than 14.8 mg g^{-1} by the MC–N. Both the removal capacities of the MC–O and MC–N are higher than that of magnetic carbon fabricated by using cotton fabric (3.73 mg g^{-1}) as the carbon precursor.[26] The larger pore size of the MC–O improved the Cr(VI) diffusion into the particles, leading to higher removal capacity. As shown in Fig. 2C and D, the pH value is an important factor affecting the Cr(VI) removal. Therefore, the Cr(VI) removal capacities by the MC–O and MC–N were also determined under acidic conditions (pH = 1.0). The Cr(VI) removal capacity of the MC–N is 327.5 mg g^{-1}, a little higher than that of MC–O (293.8 mg g^{-1}). The MC–N contains more proportion of ZVI than MC–O (Fig. 1C), which can donate more electrons for Cr(VI) reduction by the oxidation of ZVI. The smaller pore size and tight carbon layer of MC–N make the homogeneous release of electrons from the interparticles, which improve the usage efficiency of the electrons. Both the removal capacities of the MC–O and MC–N from acidic solutions are much higher than those from the neutral solutions, suggesting that the solution pH plays the most important role in the redox reaction. More protons were used for the generation of $H^{\cdot}$ and Fe^{2+}, which have been reported as widely used electron donors for Cr(VI) reduction. The removal capacities of the MC–O and MC–N under acidic conditions (pH = 1.0) are much higher than those of other carbon adsorbents, such as the magnetic carbon fabricated by rice husk (30.96 mg g^{-1}),[28] magnetic chitosan (55.8 mg g^{-1})[37] and polypyrrole–polyaniline (PPy–PANI) nanofibers (227.22 mg g^{-1}).[38] Generally, the MC–O has a better performance on Cr(VI) removal from the neutral and basic solutions, while the MC–N perform better in acidic solutions.

3.4. Cr(VI) removal mechanisms

The Cr(VI) removal mechanism was proposed considering the redox reaction and chemical precipitation in this study. Precipitants are observed in magnetic carbon nanoadsorbents after being treated with Cr(VI) (Fig. S3†). Meanwhile, Cr and Fe elements were also detected on the surface of the MC–O and MC–N by EDX (Fig. S3†). Fig. 4A shows the Cr2p XPS spectra of magnetic carbon nanoadsorbents treated with Cr(VI). The binding energy peaks at 576.85 and 587.4 eV indicate that the Cr adsorbed on the surface of adsorbents was in the form of Cr(III).[39] The result suggested that all the Cr(VI) adsorbed was totally reduced to Cr(III). The peak of Fe2p spectra (Fig. 4B) of the Cr(VI)-adsorbed magnetic carbon was deconvoluted to two major peaks at 705.3 and 709.6 eV, corresponding to ZVI and Fe^{3+}. The larger proportion of Fe^{3+} indicates that ZVI has been oxidized to Fe^{3+} by the reduction of Cr(VI). The peak of C1s spectra (Fig. 4C) was deconvoluted to two major components at 284.9 and 287.6 eV, arising from C–C and –COO, respectively. It indicates that C on the adsorbent surface was also oxidized by the Cr(VI). The O1s binding energy peaks at 531.4 and 534.5 eV (Fig. 4D), corresponding to C=O and C–O, were observed in the O1S XPS spectra. Generally, the Cr(VI) adsorbed on the adsorbents has been reduced to Cr(III) by the oxidation of both ZVI and carbon in the magnetic carbons.

Fig. 5 shows that both MC–O and MC–N exhibit good magnetic properties. The MC–O exhibits a saturation magnetization of ~53 emu g^{-1}, while the MC–N shows a larger

Published on 20 August 2014. Downloaded by University of Tennessee at Knoxville on 10/06/2016 21:53:50.

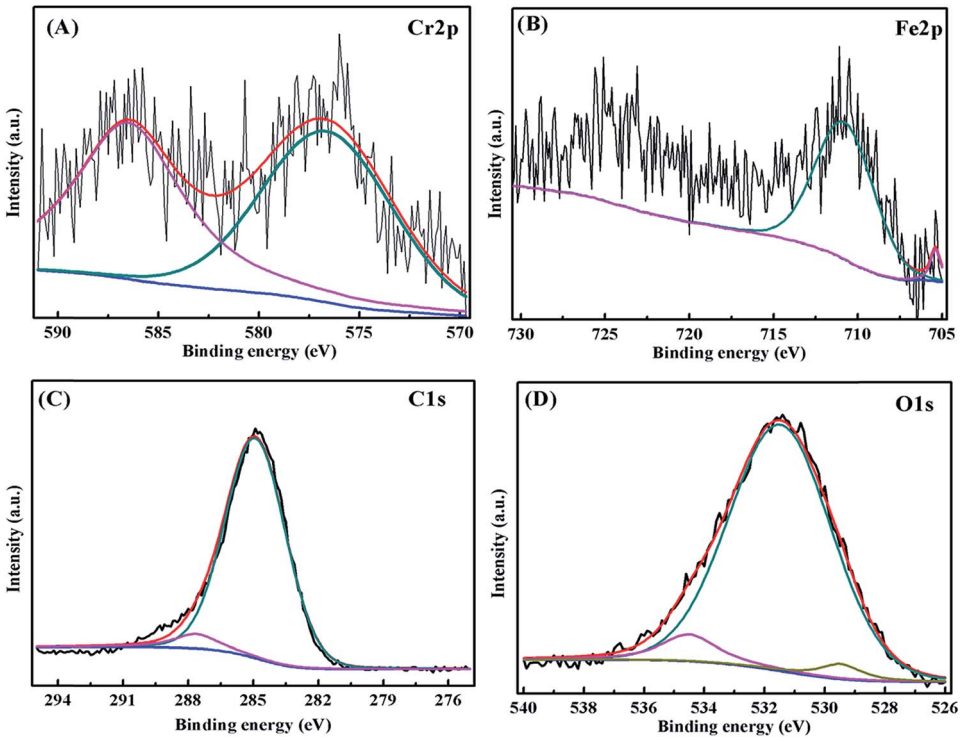

Fig. 4 (A) Cr2p, (B) Fe2p, (C) C1s and (D) O1s XPS profile of the magnetic carbon treated with 1000 mg L^{-1} Cr(VI) at initial pH 3.0.

saturation magnetization of ~61 emu g^{-1}. A little decreased saturation magnetization was observed for both MC–O and MC–N after being treated with the Cr(VI) solutions of pH 7.0, while was decreased sharply after being treated with an initial pH of 1.0, especially for the MC–N. ZVI was consumed for the Cr(VI) reduction by forming the precipitants of iron and chromium hydroxides on the adsorbent surface, leading to the decreased magnetic properties of magnetic carbon nanoadsorbents. However, the magnetic carbons also exhibit large magnetization even though they are treated with acids, which can be easily separated by a permanent magnet from the solutions after being treated (Fig. S4†).

Based on the aforementioned analysis, the Cr(VI) removal mechanisms by the magnetic carbon nanoadsorbents are schematically shown in Fig. 6. The pHs in the acidic solutions were noticed to be increased after treated with Cr(VI) (Fig. S2†), suggesting that the protons were consumed during Cr(VI) reduction. The e_{aq}^- and/or H$^\bullet$, generated from the ZVI, are likely the direct electron donors for the Cr(VI) reduction. Moreover, the Fe^{2+}, generated from the ZVI dissolving, acts as an electron donor as well. Therefore, the Cr(VI) removal from the acidic solutions by the magnetic carbon nanoadsorbents is proposed as the following reactions:

$$Fe + H^+ \rightarrow Fe^{2+} + R\ (e_{aq}^-\ \text{and/or}\ H^\bullet) \quad (5)$$

$$Cr(VI) + R \rightarrow Cr(III) \quad (6)$$

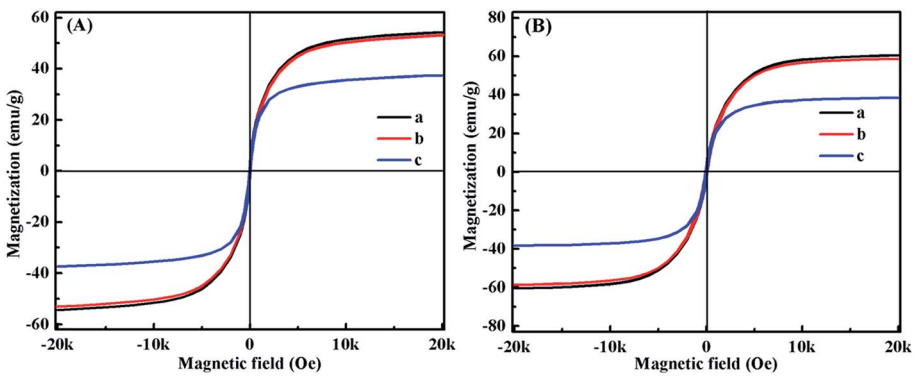

Fig. 5 (A) Magnetic hysteresis loop of the MC–O (a) before and after being treated with Cr(VI) solution at pH (b) 7.0 and (c) 1.0; (B) magnetic hysteresis loop of the MC–N (a) before and after being treated with Cr(VI) solution at pH (b) 7.0 and (c) 1.0.

 This journal is © The Royal Society of Chemistry 2014

Published on 20 August 2014. Downloaded by University of Tennessee at Knoxville on 10/06/2016 21:53:50.

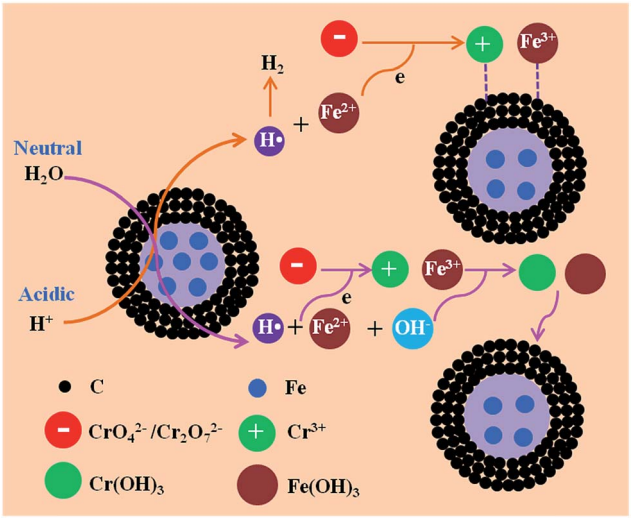

Fig. 6 Cr(VI) removal mechanism for the magnetic carbons.

$$Cr(VI) + Fe^{2+} \rightarrow Cr(III) + Fe^{3+} \quad (7)$$

$$H^{\cdot} \rightarrow H_2 \quad (8)$$

In the above reactions, R is the actual reductants for the Cr(VI) reduction, produced by ZVI. Under acidic conditions, ZVI rapidly reacts with protons and produces the reductive intermediates (eqn (5)). Then the Cr(VI) was reduced to Cr(III) by the reactive intermediates (eqn (6) and (7)). The intermediates were also scavenged by the reactive species to form H_2 (eqn (8)), which accounts for the observed bubbles in the reaction system. Finally, the Cr(III), which is positively charged, was further adsorbed onto the surface of magnetic carbons by electrostatic attraction. As shown in Fig. 3C and D, the Cr(VI) removal rate at pH 1.0 is much faster than that at pH 7.0, indicating that the redox reaction is the main mechanism involved in the Cr(VI) removal process.

However, a less increase in the pH was observed in the neutral and basic solutions after being treated by both MC–O and MC–N (Fig. S2†). Different mechanisms are involved in the Cr(VI) removal from the neutral and basic solutions (Fig. 6). Cr(VI) was reduced to Cr(III) by the oxidation of ZVI.[40] $Cr_2O_7^{2-}$ is the main form for pH higher than 6.8. Stoichiometrically, the reduction of one mol $Cr_2O_7^{2-}$ by ZVI results in the release of two mol Cr^{3+}, two mol Fe^{3+} and 14 mol hydroxide ions (OH^-) (eqn (9)). Then the Cr^{3+} and Fe^{3+} form the hydroxides and precipitate under basic conditions. The complete precipitation of the Cr^{3+} and Fe^{3+} as hydroxides and/or oxyhydroxides (eqn (10) and (11)) consumes 12 mol OH^-. Thus, the accumulation of the remaining OH^- leads to the increased pH. The complete precipitation of Cr^{3+} and Fe^{3+} on the adsorbent surface leads to complete removal of the Cr(VI) from wastewater.

$$Cr_2O_7^{2-} + Fe + H_2O \rightarrow 2Cr^{3+} + 2Fe^{3+} + 14OH^- \quad (9)$$

$$2Cr^{3+} + 6OH^- \rightarrow 2Cr(OH)_{3(s)}, \text{ or } 2Cr^{3+} + 6OH^- \rightarrow 2CrOOH_{(s)} + 2H_2O \quad (10)$$

$$2Fe^{3+} + 6OH^- \rightarrow 2Fe(OH)_{3(s)}, \text{ or } 2Fe^{3+} + 6OH^- \rightarrow 2FeOOH_{(s)} + 2H_2O \quad (11)$$

4. Conclusions

The magnetic carbon nanoadsorbents (MC–O and MC–N) derived from cellulose were fabricated through a calcination method by using the Fe_3O_4 nanoparticles and $Fe(NO_3)_3$ as the iron precursors. The MC–N has a bigger specific surface area and smaller mesopores than the MC–O. A high proportion of ZVI of the MC–N contributed to the superior performance on the Cr(VI) removal. Both the MC–O and MC–N (2.5 g L^{-1}) can remove 4.0 mg L^{-1} Cr(VI) within 10 min. The Cr(VI) removal by the magnetic carbons is highly dependent on the pH. The adsorption behaviors were fitted better with pseudo-second-order kinetics and the Langmuir isotherm model. The MC–O and MC–N have the maximum adsorption capacities of 293.8 and 327.5 mg g^{-1}, respectively. The MC–O has a better Cr(VI) removal rate and capacity than the MC–N in neutral and basic solutions, while the MC–N does better in acid solution. The Cr(VI) was reduced to Cr(III) by the reductive intermediates generated from ZVI, and then the Cr(III) was precipitated on the adsorbent surface. Moreover, the magnetic carbons can be easily separated by a permanent magnet from solutions after being treated.

Acknowledgements

This project is financially supported by Texas Hazardous Waste Research Center (THWRC) and from National Science Foundation, USA – Nanomanufacturing (CMMI 13-14486) managed by Dr Bruce M. Kramer, Nanoscale Interdisciplinary Research Team and Materials Processing and Manufacturing (CMMI 10-30755) managed by Dr Mary M. Toney and Chemical and Biological Separations (CBET 11-37441) managed by Dr Rosemarie D. Wesson. B. Qiu acknowledges the support from China Scholarship Council (CSC) program. David P. Young acknowledges support from the NSF under grant DMR 13-06392.

References

1 C. J. Lin, S. L. Wang, P. M. Huang, Y. M. Tzou, J. C. Liu, C. C. Chen, J. H. Chen and C. Lin, *Water Res.*, 2009, **43**, 5015–5022.
2 A. Qian, P. Liao, S. Yuan and M. Luo, *Water Res.*, 2014, **48**, 326–334.
3 S. Rengaraj, C. K. Joo, Y. Kim and J. Yi, *J. Hazard. Mater.*, 2003, **102**, 257–275.
4 Z. Modrzejewska and W. Kaminski, *Ind. Eng. Chem. Res.*, 1999, **38**, 4946–4950.
5 W. Liu, J. Ni and X. Yin, *Water Res.*, 2014, **53**, 12–25.
6 A. Idris, N. Hassan, N. S. Mohd Ismail, E. Misran, N. M. Yusof, A. F. Ngomsik and A. Bee, *Water Res.*, 2010, **44**, 1683–1688.

Published on 20 August 2014. Downloaded by University of Tennessee at Knoxville on 10/06/2016 21:53:50.

7 J. Zhu, S. Wei, H. Gu, S. B. Rapole, Q. Wang, Z. Luo, N. Haldolaarachchige, D. P. Young and Z. Guo, *Environ. Sci. Technol.*, 2011, **46**, 977–985.
8 C. Xu, B. Qiu, H. Gu, X. Yang, H. Wei, X. Huang, Y. Wang, D. Rutman, D. Cao and S. Bhana, *ECS J. Solid State Sci. Technol.*, 2014, **3**, M1–M9.
9 H. Gu, S. B. Rapole, Y. Huang, D. Cao, Z. Luo, S. Wei and Z. Guo, *J. Mater. Chem. A*, 2013, **1**, 2011–2021.
10 B. Qiu, C. Xu, D. Sun, H. Yi, J. Guo, X. Zhang, H. Qu, M. Guerrero, X. Wang, N. Noel, Z. Luo, Z. Guo and S. Wei, *ACS Sustainable Chem. Eng.*, 2014, **2**, 2070–2080.
11 B. Qiu, C. Xu, D. Sun, H. Wei, X. Zhang, J. Guo, Q. Wang, D. Rutman, Z. Guo and S. Wei, *RSC Adv.*, 2014, **4**, 29855–29865.
12 B. Qiu, C. Xu, D. Sun, Q. Wang, H. Gu, X. Zhang, B. L. Weeks, J. Hopper, T. C. Ho, Z. Guo and S. Wei, *Appl. Surf. Sci.*, DOI: 10.1016/j.apsusc.2014.07.039.
13 X. F. Sun, Y. Ma, X. W. Liu, S. G. Wang, B. Y. Gao and X. M. Li, *Water Res.*, 2010, **44**, 2517–2524.
14 N. Melitas, O. Chuffe-Moscoso and J. Farrell, *Environ. Sci. Technol.*, 2001, **35**, 3948–3953.
15 H. Gu, S. B. Rapole, J. Sharma, Y. Huang, D. Cao, H. A. Colorado, Z. Luo, N. Haldolaarachchige, D. P. Young and B. Walters, *RSC Adv.*, 2012, **2**, 11007–11018.
16 L. H. Zhang, Q. Sun, D. H. Liu and A. H. Lu, *J. Mater. Chem. A*, 2013, **1**, 9477–9483.
17 J. Zhu, S. Pallavkar, M. Chen, N. Yerra, Z. Luo, H. A. Colorado, H. Lin, N. Haldolaarachchige, A. Khasanov and T. C. Ho, *Chem. Commun.*, 2013, **49**, 258–260.
18 X. Zhu, Y. Liu, C. Zhou, G. Luo, S. Zhang and J. Chen, *Carbon*, 2014, **77**, 627–636.
19 P. Mitra, D. Sarkar, S. Chakrabarti and B. K. Dutta, *Chem. Eng. J.*, 2011, **171**, 54–60.
20 F. Fu, J. Ma, L. Xie, B. Tang, W. Han and S. Lin, *J. Environ. Manage.*, 2013, **128**, 822–827.
21 L. n. Shi, X. Zhang and Z.-l. Chen, *Water Res.*, 2011, **45**, 886–892.
22 S. Wei, Q. Wang, J. Zhu, L. Sun, H. Lin and Z. Guo, *Nanoscale*, 2011, **3**, 4474–4502.
23 H. Gu, D. Ding, P. Sameer, J. Guo, N. Yerra, Y. Huang, Z. Luo, T. C. Ho, N. Haldolaarachchige and D. P. Young, *Electrochem. Solid-State Lett.*, 2013, **2**, M65–M68.
24 T. Liu, Z. L. Wang, X. Yan and B. Zhang, *Chem. Eng. J.*, 2014, **245**, 34–40.
25 V. Nahuel Montesinos, N. Quici, E. Beatriz Halac, A. G. Leyva, G. Custo, S. Bengio, G. Zampieri and M. I. Litter, *Chem. Eng. J.*, 2014, **244**, 569–575.
26 J. Zhu, H. Gu, J. Guo, M. Chen, H. Wei, Z. Luo, H. A. Colorado, N. Yerra, D. Ding, T. C. Ho, N. Haldolaarachchige, J. Hopper, D. P. Young, Z. Guo and S. Wei, *J. Mater. Chem. A*, 2014, **2**, 2256–2265.
27 J. D. Xiao, L. G. Qiu, X. Jiang, Y. J. Zhu, S. Ye and X. Jiang, *Carbon*, 2013, **59**, 372–382.
28 Y. Li, S. Zhu, Q. Liu, Z. Chen, J. Gu, C. Zhu, T. Lu, D. Zhang and J. Ma, *Water Res.*, 2013, **47**, 4188–4197.
29 X. Qi, L. Li, T. Tan, W. Chen and R. L. Smith, *Environ. Sci. Technol.*, 2013, **47**, 2792–2798.
30 M. Sevilla and A. B. Fuertes, *Carbon*, 2009, **47**, 2281–2289.
31 X. He, J. A. Lie, E. Sheridan and M. B. Hägg, *Ind. Eng. Chem. Res.*, 2011, **50**, 2080–2087.
32 A. M. Ruppert, M. Niewiadomski, J. Grams and W. Kwapiński, *Appl. Catal., B*, 2014, **145**, 85–90.
33 G. Wen, Y. Xu, Z. Xu and Z. Tian, *Catal. Commun.*, 2010, **11**, 522–526.
34 Y. Wu, X. Ma, M. Feng and M. Liu, *J. Hazard. Mater.*, 2008, **159**, 380–384.
35 E. Álvarez-Ayuso, A. García-Sánchez and X. Querol, *Water Res.*, 2003, **37**, 4855–4862.
36 R. Sudha Bai and T. E. Abraham, *Bioresour. Technol.*, 2003, **87**, 17–26.
37 N. N. Thinh, P. T. B. Hanh, L. T. T. Ha, L. N. Anh, T. V. Hoang, V. D. Hoang, L. H. Dang, N. V. Khoi and T. D. Lam, *Mater. Sci. Eng., C*, 2013, **33**, 1214–1218.
38 M. Bhaumik, A. Maity, V. V. Srinivasu and M. S. Onyango, *Chem. Eng. J.*, 2012, **181–182**, 323–333.
39 D. Park, Y.-S. Yun and J. M. Park, *J. Colloid Interface Sci.*, 2008, **317**, 54–61.
40 K. C. K. Lai and I. M. C. Lo, *Environ. Sci. Technol.*, 2008, **42**, 1238–1244.

 This journal is © The Royal Society of Chemistry 2014